Acta Crystallographica Section D
Biological Crystallography
ISSN 0907-4449

The structure of L-amino-acid ligase from *Bacillus licheniformis*

Michihiko Suzuki,[a] Yuichi Takahashi,[a] Atsushi Noguchi,[b] Toshinobu Arai,[b] Makoto Yagasaki,[c] Kuniki Kino[b] and Jun-ichi Saito[a]*

[a]Drug Discovery Research Laboratories, Kyowa Hakko Kirin Co. Ltd, 1188 Shimotogari, Nagaizumi-cho, Sunto-gun, Shizuoka 411-8731, Japan, [b]Department of Applied Chemistry, Faculty of Science and Engineering, Waseda University, 3-4-1 Ohkubo, Shinjuku-ku, Tokyo 169-8555, Japan, and [c]Technical Research Laboratories, Hofu Yamaguchi Production Center, Kyowa Hakko Bio Co. Ltd, 1-1 Kyowa-cho, Hofu-shi, Yamaguchi 747-8522, Japan

Correspondence e-mail: jun.saito@kyowa-kirin.co.jp

Received 13 March 2012
Accepted 5 September 2012

PDB Reference: L-amino-acid ligase, 3vot

L-Amino-acid ligases (LALs) are enzymes which catalyze the formation of dipeptides by linking two L-amino acids. Although many dipeptides are known and expected to have medical and nutritional benefits, their practical use has been limited owing to their low availability and high expense. LALs are potentially desirable tools for the efficient production of dipeptides; however, the molecular basis of substrate recognition by LAL has not yet been sufficiently elucidated for the design of ideal LALs for the desired dipeptides. This report presents the crystal structure of the LAL BL00235 derived from *Bacillus licheniformis* NBRC 12200 determined at 1.9 Å resolution using the multi-wavelength anomalous dispersion method. The overall structure of BL00235 is fairly similar to that of YwfE, the only LAL with a known structure, but the structure around the catalytic site contains some significant differences. Detailed structural comparison of BL00235 with YwfE sheds some light on the molecular basis of the substrate specificities.

1. Introduction

Dipeptides are substances that consist of two amino acids connected by a peptide bond. Although amino acids themselves have various physiological activities, dipeptides are expected to reinforce or alter their original physiological activities or to reveal improved physicochemical properties. For example, L-glutamine (Gln) is employed as an important nutrient in various healthcare applications. Its practical use, however, has been limited owing to its instability in solution. Transformation of Gln into the dipeptide L-alanyl-L-glutamine (Ala-Gln) drastically improves its stability in solution (Fürst, 2001). Despite their many potential benefits, usage of dipeptides has been limited owing to a lack of efficient production processes.

Recently, L-amino-acid ligases (LALs; EC 6.3.2.28) were discovered to be novel ATP-grasp superfamily enzymes that catalyze the formation of an α-peptide bond between two L-amino acids in an ATP-dependent manner (Tabata *et al.*, 2005; Kino, Nakazawa *et al.*, 2008; Kino, Noguchi *et al.*, 2008). ATP-grasp superfamily proteins are ATP-dependent carboxylase-amine/thiol ligases that possess an atypical ATP-binding motif characterized by two $\alpha+\beta$ domains referred to as the ATP-grasp fold. The members of this family share a common structural architecture that consists of three domains referred to as the A-domain, B-domain and C-domain. The C-domain can be further divided into the C1-subdomain and the C2-subdomain (Figs. 1*a* and 1*b*; Fawaz *et al.*, 2011), although some enzymes lack the C2-subdomain, as is observed in D-alanine:D-alanine ligase (DDL; Fig. 1*c*; Fan *et al.*, 1994).

Application of LALs to dipeptide production is advantageous because the reaction is unidirectional and does not require any complicated procedures such as protection or derivatization of the substrates. Despite these advantages, the application of LALs to the production of various dipeptides has remained difficult owing to their substrate specificity. Furthermore, the lack of three-dimensional structures of LALs has made it difficult to design LALs using protein engineering to obtain desirable substrate specificities. Very recently, the three-dimensional structure of YwfE, the first identified LAL, has been solved in complex with a substrate analogue (Shomura *et al.*, 2012). The structure of YwfE revealed that the binding mode of the substrate analogue to YwfE is the opposite of that expected from the crystal structure of DDL: the N-terminal amino acid of the dipeptide initially binds to the inner side of the substrate-binding pocket and the second, C-terminal, amino acid then binds at the lid of the pocket.

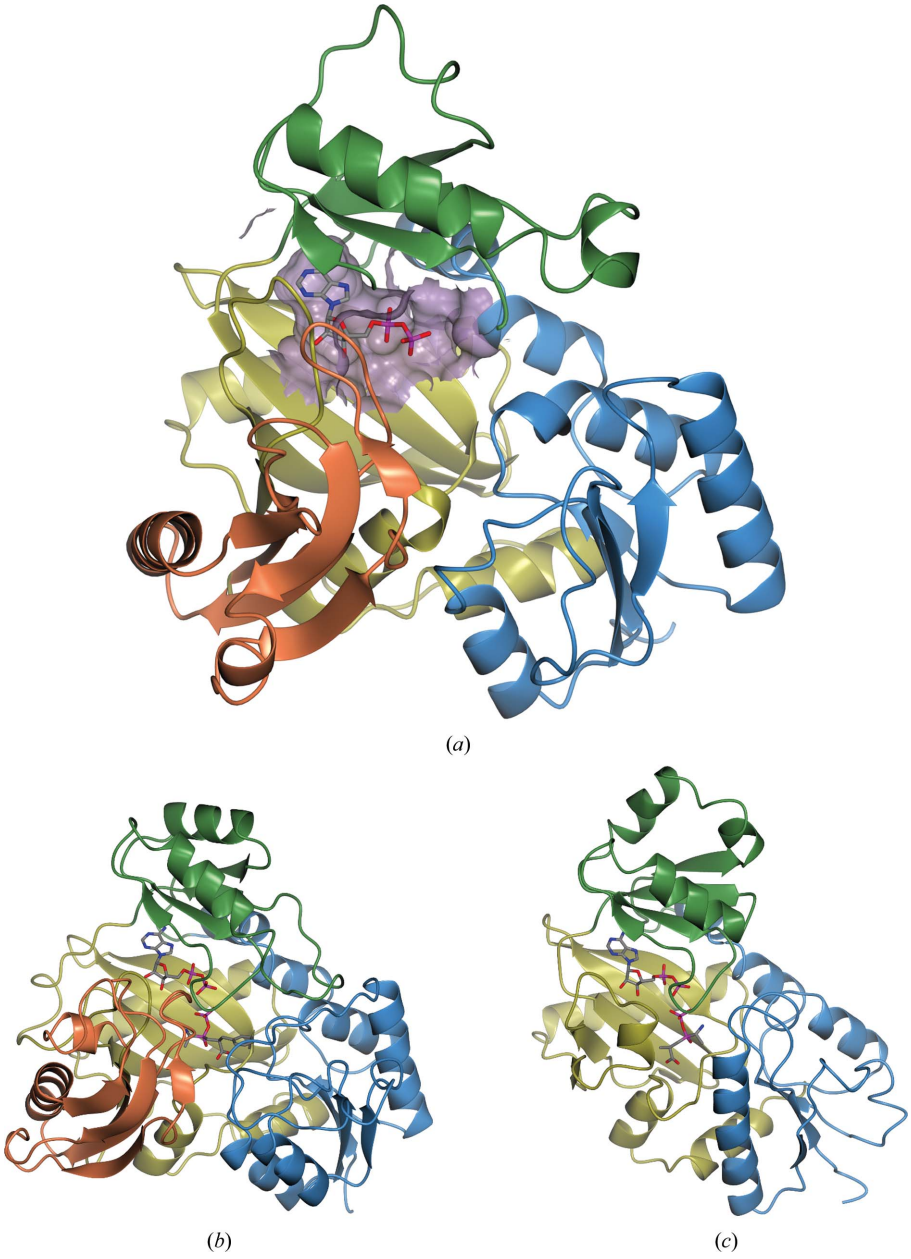

Figure 1
Comparison of the overall structure of BL00235 with other amino-acid ligases. (*a*) Ribbon diagram of the overall BL00235 structure in complex with ADP. The A-domain, B-domain, C1-domain and C2-domain are represented in blue, green, gold and orange, respectively. The ATP/substrate-binding pocket is shown as a purple surface. The ADP molecule is shown as a stick model, with C, N, O and P atoms coloured grey, blue, red and magenta, respectively. (*b*) The structure of YwfE (PDB entry 3vmm; Shomura *et al.*, 2012). The A-domain, B-domain, C1-domain and C2-domain are shown in the same colours as for BL00235 in (*a*). (*c*) The structure of DDL from *E. coli* (PDB entry 2dln; Fan *et al.*, 1994). The A-domain, B-domain and C-domain are shown in blue, green and gold, respectively.

BL00235 from *Bacillus licheniformis* NBRC 12200 is an LAL found as a homologous protein to the previously found LALs YwfE and RSp1486a. YwfE and RSp1486a have a rather wide range of substrate specificity (Tabata *et al.*, 2005; Kino, Nakazawa *et al.*, 2008). BL00235, in contrast, has a highly restricted substrate specificity: the N-terminal substrate is confined to L-methionine and L-leucine, while the C-terminal substrates include small residues such as L-alanine, L-serine, L-threonine and L-cysteine (Kino, Noguchi *et al.*, 2008).

A crystallographic analysis of BL00235 was performed to investigate the molecular basis of its restricted substrate specificity.

2. Materials and methods

2.1. Expression and purification

The BL00235 gene (GenBank accession No. CP000002) was amplified from genomic DNA of *B. licheniformis* NBRC12200 by the polymerase chain reaction (PCR) using the following primers: sense, 5′-AAGGGAAACATATGACGAAACGAAACAAAAACTTG-3′ (*Nde*I), and antisense, 5′-AAAGGATCCTTAACCTCCTATTGTACCCGTC-3′ (*Bam*HI). The PCR fragment was digested with the restriction enzymes and ligated into pET-21a(+) vector. The resulting plasmid was designed to express the gene without any affinity-tag sequences. The plasmid was introduced into *Escherichia coli* BL21(DE3) and *E. coli* B834(DE3) by electroporation.

Recombinant *E. coli* BL21(DE3) cells were cultivated in LB medium (1% Bacto tryptone, 0.5% yeast extract, 1% NaCl) containing 50 µg ml^{-1} ampicillin (final concentration) to produce native

BL00235 protein. Recombinant *E. coli* B834(DE3) cells were cultivated in LeMaster medium (LeMaster & Richards, 1985) containing 50 μg ml^{-1} ampicillin (final concentration) to produce selenomethionine-substituted BL00235 protein. Gene expression was induced by the addition of isopropyl β-D-1-thiogalactopyranoside (final concentration 0.1 m*M*) at an OD_{660} of 0.5–0.7. The cultivated cells were harvested by centrifugation (4160*g*, 10 min, 277 K), resuspended in 50 m*M* Tris–HCl buffer pH 8.0 and disrupted by sonication at 277 K. Cellular debris was removed by centrifugation (17 000*g*, 30 min, 277 K) and the supernatant was collected as a cell-free extract.

Both native and SeMet-substituted BL00235 proteins were purified using the same procedure. All purification procedures were performed at 277 K or on ice and each active fraction was filtered using a cellulose acetate membrane (0.45 μm pore size; Advantec, Tokyo, Japan). The cell-free extract was loaded onto a Toyopearl DEAE 650S column (Tosoh, Tokyo, Japan) previously equilibrated with 50 m*M* Tris–HCl buffer pH 8.0 and the column was washed with the same buffer. The protein was eluted with a linear gradient of 0–0.25 *M* KCl at a flow rate of 2 ml min^{-1}. The active fractions were collected and ammonium sulfate was added to prepare a protein solution containing 1.5 *M* ammonium sulfate. The protein solution was then loaded onto a HiPrep Phenyl HP column (GE Healthcare, Buckinghamshire, England) previously equilibrated with 50 m*M* Tris–HCl buffer pH 8.0 containing 1.5 *M* ammonium sulfate and the column was washed with the same buffer. The enzyme was eluted with a linear gradient of 1.5–0 *M* ammonium sulfate at a flow rate of 1.5 ml min^{-1}. The active fractions were collected and dialyzed against 50 m*M* Tris–HCl buffer pH 8.0. The resulting protein solution was then loaded onto a Mono Q 5/50 GL column (GE Healthcare) previously equilibrated with 50 m*M* Tris–HCl buffer pH 8.0 and the column was washed with the same buffer. The protein was eluted with a linear gradient of 0–0.3 *M* KCl at a flow rate of 1 ml min^{-1}. The active fractions were collected and concentrated by ultrafiltration. Finally, the protein solution was loaded onto a HiLoad 16/60 Superdex 200pg column (GE Healthcare) previously equilibrated with 50 m*M* Tris–HCl buffer pH 8.0 containing 5 m*M* dithiothreitol (DTT). The enzyme was eluted with the same buffer at a flow rate of 0.5 ml min^{-1} and the active fractions were collected and concentrated by ultrafiltration. Consequently, purified BL00235 protein was obtained at 8 mg ml^{-1} and was detected as a single band on SDS–PAGE.

2.2. Crystallization and data collection

Native and SeMet-substituted BL00235 were crystallized under similar conditions. The crystals of BL00235 were grown at room temperature using the sitting-drop vapour-diffusion method. The crystallization droplet consisted of 1 μl protein solution (consisting of 8 mg ml^{-1} protein, 1.6 m*M* ADP, 1.6 m*M* Met-Ala dipeptide) and 1 μl reservoir solution [100 m*M* $CaCl_2$, 24–27%(*w*/*v*) PEG MME 550, 4%(*v*/*v*) 2-propanol in 100 m*M* imidazole pH 6.5] and was equilibrated against 300 μl reservoir solution. Rod-shaped crystals belonging to the orthorhombic space group $P2_12_12_1$ with two enzyme molecules per asymmetric unit appeared after several days. The Matthews coefficient and solvent content of the crystals were 2.1 Å^3 Da^{-1} and 41.5%, respectively. The crystals were flash-cooled in liquid nitrogen after immersion in a cryoprotection solution containing 15%(*v*/*v*) glycerol. Native and multi-wavelength X-ray diffraction data sets were collected on the X06SA beamline at the Swiss Light Source (SLS), Paul Scherrer Institut (PSI).

Table 1
Data-collection and refinement statistics.

Values in parentheses are for the highest resolution shell.

		SeMet		
	Native	Peak	Edge	Remote
Data collection				
Beamline	X06SA, SLS	X06SA, SLS		
Wavelength (Å)	1.00000	0.97920	0.97970	0.97200
Space group	$P2_12_12_1$	$P2_12_12_1$		
Unit-cell parameters	*a* = 58.09, *b* = 90.03, *c* = 154.91	*a* = 57.90, *b* = 89.66, *c* = 154.15		
Mosaicity (°)	0.43	0.183		
Resolution range (Å)	30.0–1.9	48.6–1.6	48.6–1.6	48.7–1.6
Observed reflections	355696	611893	594351	613565
Unique reflections	63092	106587	106452	106849
Average multiplicity†	5.6 (5.5)	2.9 (2.6)	2.9 (2.6)	2.9 (2.7)
Completeness† (%)	97.4 (91.7)	97.6 (94.4)	97.1 (94.6)	97.5 (95.5)
R_{merge} (%)	11.5 (73.6)	10.5 (71.7)	8.9 (63.7)	10.9 (106.5)
$\langle I/\sigma(I)\rangle$	11.0 (2.3)	15.2 (1.2)	16.1 (1.5)	14.2 (0.8)
Refinement				
Resolution range (Å)	29.5–1.9			
No. of reflections	59906			
R_{cryst}/R_{free} (%)	19.0/23.6			
No. of atoms				
Protein	6369			
Ligands	78			
Water	632			
R.m.s. deviations				
Bond lengths (Å)	0.007			
Bond angles (°)	1.16			
B factors (Å^2)				
Protein	30.5			
Ligands	35.0			
Water	32.8			
Ramachandran plot (%)				
Most favoured	92.3			
Additional allowed	7.3			
Generously allowed	0.1			
Disallowed	0.3			

† Bijvoët mates were treated as non-equivalent for MAD data.

2.3. Structure determination

The multi-wavelength X-ray diffraction data were processed using the *XDS* program package (Kabsch, 2010). Ten Se-atom sites were found by the program *SOLVE* (Terwilliger & Berendzen, 1999) using data to 2.3 Å resolution. Phase improvement was performed by solvent flattening and NCS averaging using the program *RESOLVE* (Terwilliger, 2000). The phases were extended to 1.6 Å resolution, resulting in a high-quality electron-density map that was sufficient to build a model of about 70% of the residues

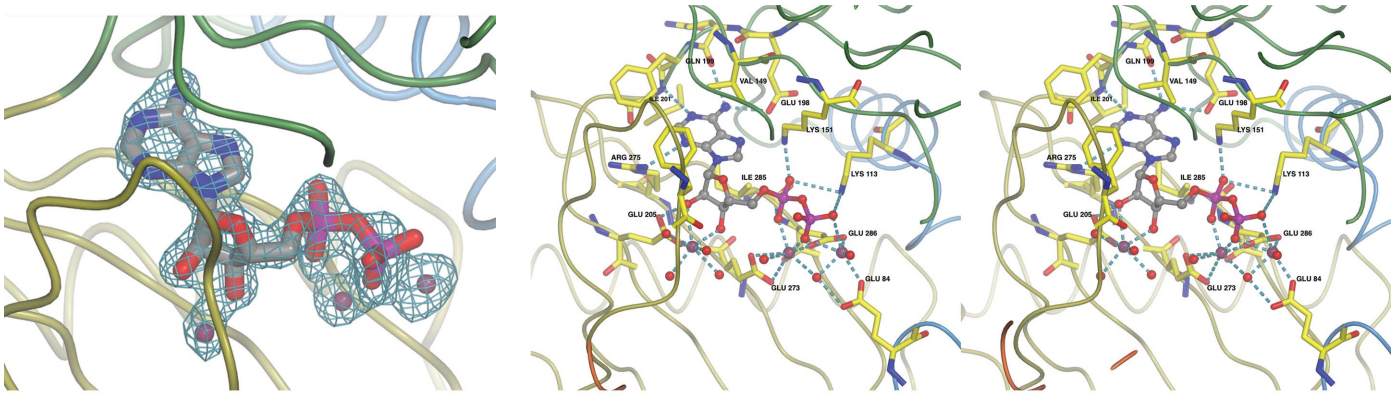

(*a*) (*b*)

Figure 2
Structural details of the ATP-binding site. (*a*) The electron-density map of an ADP molecule bound to BL00235 and three calcium ions coordinating ADP. The $F_o - F_c$ electron-density OMIT map was calculated using the ligand-free model and is represented as a mesh coloured dark cyan at a contour level of 3.0σ. The ADP molecule is shown as a thick stick model and three calcium ions are shown as purple balls. BL00235 is represented as tubes tracing its C^α atoms in the same domain colours as in Fig. 1. (*b*) Stereo diagram of interactions between ADP and BL00235. ADP bound to BL00235 is shown as a ball-and-stick model with its C atoms in grey. The calcium ions coordinating ADP are shown as purple balls. The surrounding residues of BL00235 are shown as sticks with C atoms in yellow. The hydrogen bonds and ion coordination are indicated as broken lines coloured light blue.

automatically with *RESOLVE* (Terwilliger, 2003). The native data set was processed using *MOSFLM* (Leslie, 1992) and scaled using *SCALA* (Evans, 2006) within the *CCP*4 program suite (Winn *et al.*, 2011). Molecular replacement was performed with *MOLREP* (Vagin & Teplyakov, 2010) to obtain the initial phases for the native data set using the SeMet-substituted BL00235 structure as a search model. The remaining residues, ADP, calcium ions and ordered water molecules were modelled into the electron-density map using *Coot* (Emsley *et al.*, 2010). Refinement of the model for the native data set was carried out using *CNX* (Brünger *et al.*, 1998) and *REFMAC* (Murshudov *et al.*, 2011). The final model of native BL00235 consisted of 805 of the 850 amino-acid residues of two monomers, two ADP molecules, nine calcium ions and 632 water molecules. The values of R_{cryst} and R_{free} converged to 19.0% and 23.6%, respectively, for the native data set at 1.9 Å resolution. The Ramachandran plot shows that almost all of the main-chain dihedral angles of nonglycine residues fall into the favoured (92.3%) or additionally allowed (7.3%) regions. The data-collection and refinement statistics are listed in Table 1. Figures were generated with *CCP*4*mg* (McNicholas *et al.*, 2011).

3. Results and discussion

3.1. Overall structure

BL00235 consists of three $\alpha+\beta$ domains referred to as the A-domain (Thr2–Asn123), the B-domain (Gly124–Phe200) and the C-domain (Ile201–Asn417), as in other ATP-grasp superfamily proteins; the C-domain is composed of the C1-subdomain (Ile201–Arg334) and the C2-subdomain (Thr335–Asn417). BL00235 has a deep embedded substrate-binding pocket that captures ATP at the bottom of the pocket (Fig. 1*a*). The A-domain of BL00235 is composed of six strands, four of which form a parallel β-sheet flanked by two and one α-helices. Two additional helices that are orthogonal to each other and connected *via* Asn112 provide a linkage between the A-domain and the B-domain. This motif, referred to as helix–residue–helix, is characteristic of ATP-grasp superfamily proteins (Thoden *et al.*, 1999). The small B-domain is comprised of a four-stranded antiparallel β-sheet and two helices covering one side of the β-sheet. The large C-domain covers one side of the embedded substrate-binding pocket and is composed of an eight-stranded twisted antiparallel β-sheet as a scaffold. The five α-helices are located on both sides of the large β-sheet. An additional three-stranded antiparallel β-sheet exists at the limb of the substrate-binding pocket. The overall structure of BL00235 is highly similar to that of YwfE (Fig. 1*b*): the root-mean-square difference (r.m.s.d.) between 372 corresponding C^α atoms of the two enzymes is 2.71 Å, although the sequence identity is low (∼20%; Supplementary Fig. S1[1]). The BL00235 structure is also very similar to that of DDL, apart from the C-terminal C2-subdomain, which does not exist in DDL (Fig. 1*c*): the r.m.s.d. is 2.07 Å for 239 corresponding C^α atoms.

3.2. Structure of the ATP-binding site

The electron-density map clearly shows that an ADP molecule is located at the bottom of the substrate-binding pocket, flanked by the B-domain and the C-domain (Fig. 2*a*). Fig. 2(*b*) shows the interactions between ADP, calcium ions and BL00235. Three calcium ions from the the crystallization mother liquor were found to coordinate the ADP through the O atoms in the ribose moiety and the α-phosphate and β-phosphate. These calcium ions could be artifacts, given the crystallization conditions. However, it is likely that the two phosphate-coordinating calcium ions mimic the physiological

[1] Supplementary material has been deposited in the IUCr electronic archive (Reference: BE5205). Services for accessing this material are described at the back of the journal.

magnesium ions coordinating the ADP. The positions of these calcium ions are equivalent to those of physiological magnesium ions in other enzymes of the ADP-grasp family (Fan *et al.*, 1994; Thoden *et al.*, 1999; Shomura *et al.*, 2012). The adenine ring is anchored to the protein by forming hydrogen bonds to the η-amino group of Arg275, the δ-carboxyl group of Glu198 and the peptide carbonyl and NH groups of Gln199 and Ile201, respectively. The 2′- and 3′-hydroxyl groups of the ribose moiety coordinate a calcium ion with distances of 2.8 and 2.3 Å, respectively. One of the carboxyl O atoms of Glu205 coordinates the calcium ion, while the other carboxyl O atom forms hydrogen bonds to the 2′-hydroxyl group of the ribose moiety. The α-phosphoryl and β-phosphoryl groups are recognized by two lysine residues: Lys151 and Lys113, respectively. The region from Phe156 to Gly160, which is implicated in the interaction with the γ-phosphate of ATP in other ATP-grasp proteins, is disordered in the BL00235 crystal structure owing to the absence of the γ-phosphate. The two phosphate-coordinating calcium ions are stabilized by Glu273, Glu84, Glu286 and surrounding water molecules, forming an octahedral coordination.

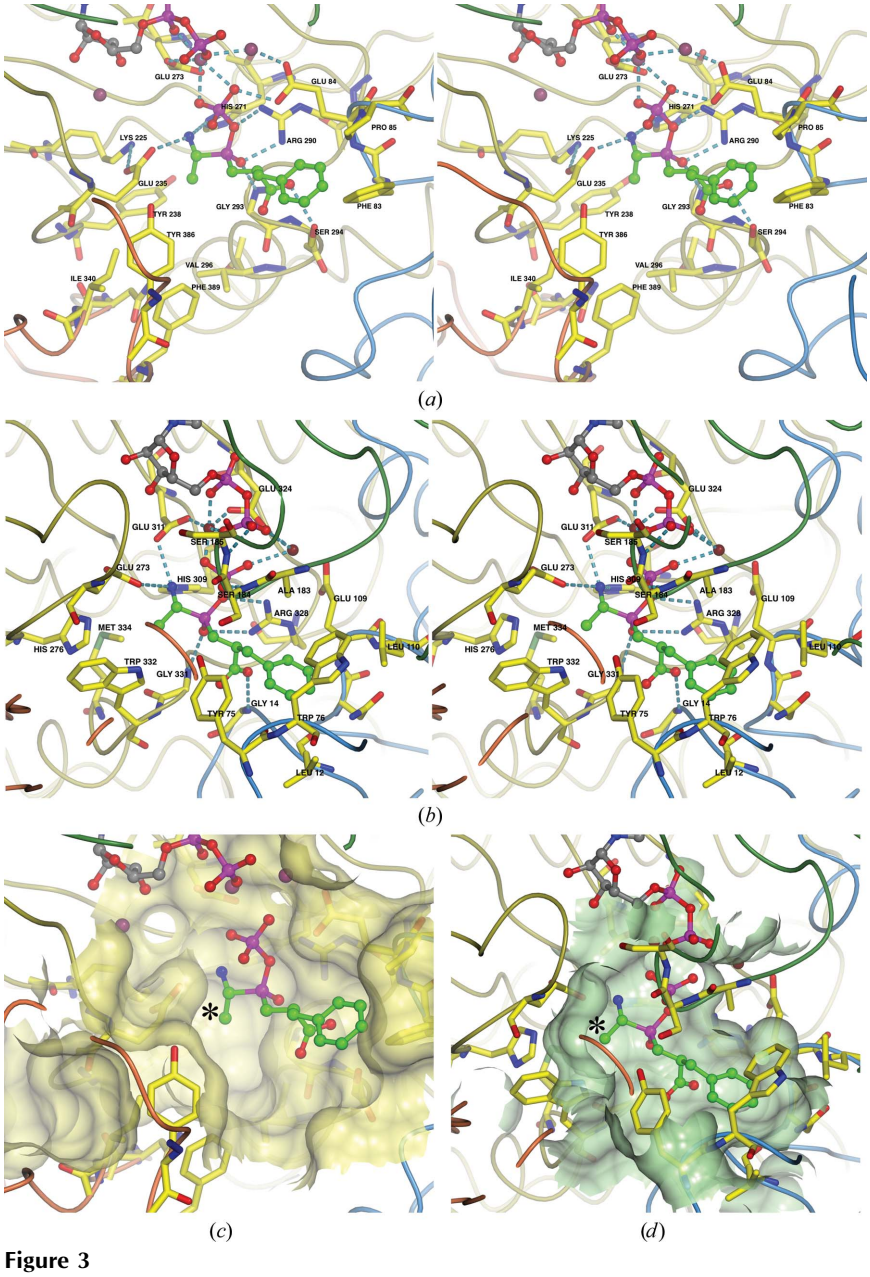

Figure 3
Structure comparison of the catalytic sites in BL00235 and YwfE. (*a*) Stereo diagram of the superimposed model structure of the BL00235–PP transition-state analogue complex. The superimposed PP analogue is shown as a ball-and-stick model with C atoms in green. Protein residues surrounding the PP analogue are shown as stick models with C atoms in yellow. Putative interactions are indicated by broken lines coloured light blue. (*b*) Stereo diagram of the structure of the YwfE–PP transition-state analogue complex. The PP analogue molecule bound to YwfE is shown as a ball-and-stick model with C atoms in green. Protein residues surrounding the PP analogue are shown as stick models with C atoms in yellow. The hydrogen bonds are indicated by broken lines coloured light blue. (*c*) Surface representation of the substrate-binding pocket of BL00235. An asterisk indicates the N-terminal C^{β} atom of the superimposed PP analogue. (*d*) Surface representation of the substrate-binding pocket of YwfE. An asterisk indicates the N-terminal C^{β} atom of the PP analogue bound to YwfE.

3.3. Structure of the dipeptide-binding site

Comparisons with YwfE suggest that the dipeptide-binding site is located at the top of the deep substrate-binding pocket organized by the A-domain and the C-domain. Although a weak blob of electron density was found near the dipeptide-binding site, it was not sufficiently clear to conclude that the density corresponded to the Met-Ala dipeptide that was added to the crystallization drop (Supplementary Fig. S2). The structure of YwfE in complex with the phosphinophosphate (PP) transition-state analogue (PDB entry 3vmm; Shomura *et al.*, 2012) was superimposed onto the BL00235 crystal structure to evaluate the substrate recognition and specificity of BL00235. The superimposed PP analogue provides an appropriate model of substrate-bound structure of BL00235. Arg290 and Gly293, which are highly conserved in LALs (Supplementary Fig. S1), are located in a position suitable for stabilizing the high-energy tetrahedral intermediate of amino-acid ligation (Fig. 3*a*). This suggests that the superimposed model is appropriate for discussion of the substrate-bound structure of BL00235 as well as to conclude that Arg290 and Gly293 are critical residues for enzymatic activity. The superimposed model indicates that Glu235 and His271, which are conserved in YwfE, are responsible for recognition of the N-terminal amino group of the substrate. On the other hand, the C-terminal carboxyl group is positioned for recognition by Ser294 of the C-domain. This

interaction is not conserved in YwfE, in which the carboxyl group interacts with Gly14 of the A-domain (Figs. 3*a* and 3*b*). Tyr238, Val296, Ile340, Tyr386 and Phe389 form a hydrophobic cavity around C^{β} of the N-terminal alanine of the analogue in the substrate-bound model of BL00235 (Figs. 3*a* and 3*c*). The existence of this extensive hydrophobic cavity provides a good explanation for the N-terminal amino-acid specificity of BL00235, which is restricted to L-methionine or L-leucine. This hydrophobic cavity is filled with the bulky hydrophobic side chains of Trp332 and Met334 in the YwfE structure (Figs. 3*b* and 3*d*), consistent with the N-terminal preference of YwfE for small residues such as glycine, L-alanine, L-serine and L-threonine. In contrast, as there is no C2-subdomain residue directly associated with substrate recognition in YwfE, Ile340, Tyr386 and Phe389 in the C2-subdomain are considered to contribute to the recognition of the N-terminal substrate in BL00235.

The recognition of the C-terminal substrate in BL00235 is less clear because the loop between Gly155 and Val166 was disordered in our structure. The loop corresponds to Loop5 near the C-terminal phenylalanine of the substrate analogue in YwfE (Shomura *et al.*, 2012). However, the superposed C-terminal phenylalanine in the PP analogue is too close to Phe83 and Pro85 of BL00235 (Fig. 3*a*). These residues possibly determine the C-terminal preference of BL00235 for smaller residues including L-alanine and L-serine. Furthermore, the bulky Phe156 in Loop5 of BL00235 may be relevant to the C-terminal substrate specificity, as its corresponding residue Ala183 in YwfE makes hydrophobic contacts with the C-terminal phenylalanine (Fig. 3*b*).

In summary, the high-resolution crystal structure of BL00235 revealed structural details of the substrate-binding pocket. The molecular mechanism of the substrate recognition of BL00235 is proposed by comparison with the previously solved structure of YwfE. These findings should be helpful in engineering LALs that possess desirable substrate specificities.

We thank Dr Yoshiyuki Yonetani and Dr Taiji Oashi for critically reading the manuscript and for useful comments.

References

Brünger, A. T., Adams, P. D., Clore, G. M., DeLano, W. L., Gros, P., Grosse-Kunstleve, R. W., Jiang, J.-S., Kuszewski, J., Nilges, M., Pannu, N. S., Read, R. J., Rice, L. M., Simonson, T. & Warren, G. L. (1998). *Acta Cryst.* D**54**, 905–921.
Emsley, P., Lohkamp, B., Scott, W. G. & Cowtan, K. (2010). *Acta Cryst.* D**66**, 486–501.
Evans, P. (2006). *Acta Cryst.* D**62**, 72–82.
Fan, C., Moews, P. C., Walsh, C. T. & Knox, J. R. (1994). *Science*, **266**, 439–443.
Fawaz, M. V., Topper, M. E. & Firestine, S. M. (2011). *Bioorg. Chem.* **39**, 185–191.
Fürst, P. (2001). *J. Nutr.* **131**, 2562S–2568S.
Kabsch, W. (2010). *Acta Cryst.* D**66**, 125–132.
Kino, K., Nakazawa, Y. & Yagasaki, M. (2008). *Biochem. Biophys. Res. Commun.* **371**, 536–540.
Kino, K., Noguchi, A., Nakazawa, Y. & Yagasaki, M. (2008). *J. Biosci. Bioeng.* **106**, 313–315.
LeMaster, D. M. & Richards, F. M. (1985). *Biochemistry*, **24**, 7263–7268.
Leslie, A. G. W. (1992). *Jnt CCP4/ESF–EACBM Newsl. Protein Crystallogr.* **26**.
McNicholas, S., Potterton, E., Wilson, K. S. & Noble, M. E. M. (2011). *Acta Cryst.* D**67**, 386–394.
Murshudov, G. N., Skubák, P., Lebedev, A. A., Pannu, N. S., Steiner, R. A., Nicholls, R. A., Winn, M. D., Long, F. & Vagin, A. A. (2011). *Acta Cryst.* D**67**, 355–367.
Shomura, Y., Hinokuchi, E., Ikeda, H., Senoo, A., Takahashi, Y., Saito, J., Komori, H., Shibata, N., Yonetani, Y. & Higuchi, Y. (2012). *Protein Sci.* **21**, 707–716.
Tabata, K., Ikeda, H. & Hashimoto, S. (2005). *J. Bacteriol.* **187**, 5195–5202.
Terwilliger, T. C. (2000). *Acta Cryst.* D**56**, 965–972.
Terwilliger, T. C. (2003). *Acta Cryst.* D**59**, 38–44.
Terwilliger, T. C. & Berendzen, J. (1999). *Acta Cryst.* D**55**, 849–861.
Thoden, J. B., Kappock, T. J., Stubbe, J. & Holden, H. M. (1999). *Biochemistry*, **38**, 15480–15492.
Vagin, A. & Teplyakov, A. (2010). *Acta Cryst.* D**66**, 22–25.
Winn, M. D. *et al.* (2011). *Acta Cryst.* D**67**, 235–242.